Journal of Sound and Vibration (1999) **225**(4), 767–778
Article No. jsvi.1999.2302, available online at http://www.idealibrary.com on IDEAL®

THE INFLUENCE OF TORSION ON ROTOR/STATOR CONTACT IN ROTATING MACHINERY

S. EDWARDS, A. W. LEES AND M. I. FRISWELL

Department of Mechanical Engineering, University of Wales Swansea, Swansea, SA2 8PP, Wales

(*Received* 9 *December* 1998, *and in final form* 8 *April* 1999)

The phenomenon of contact between a rotor and its stator, known as rub, has long been recognized as a serious cause of failure in rotating machinery. The analysis of rub is particularly complex, due to non-linear and often chaotic behaviour. Numerical simulation is the preferred method of analysis and, due to improvements in digital computing in recent years, it has become possible to analyze ever-more complex numerical models. To this end, the analysis of rotor/stator contact has seen a corresponding increase in the amount of research invested in it. One aspect of the dynamics involved with the occurrence of rub that has not been investigated until now, is that of the effects of torsion. In the literature, steady state analysis is limited to lateral movement: this paper includes torsional effects in a rotor/stator contact model and highlights the importance of its inclusion by way of a numerical example having realistic physical parameters.

1. INTRODUCTION

Unwanted contact between the rotating and stationary parts of a rotating machine, more commonly referred to as rub, is a serious problem that has been regularly identified as a primary mode of failure in rotating machinery. Rub may typically be caused by mass imbalance, turbine or compressor blade failure, defective bearings and/or seals, or by rotor misalignment, either thermal or mechanical. It is therefore surprising that the quantity of research undertaken concerning this not-uncommon rotor-dynamic problem is indeed small, in comparison with some of the better-understood faults encountered in this area, such as mass unbalance or cracked shafts. On closer inspection, however, one finds that the reason for this discrepancy is likely to be the intrinsically complicated nature of the problem. Several different physical events may occur during a period of contact between rotor and stator: initial impacting stage, frictional behaviour between the two contacting parts and an increase in the stiffness of the rotating system whilst contact is maintained, to name just three. The behaviour of the system during this period is highly non-linear and may be chaotic.

During the last two decades, the majority of research undertaken in this area has been centred on the development and refinement of mathematical models, to allow

0022-460X/99/340767 + 12 $30.00/0

the rubbing phenomenon to be more accurately understood. For a detailed overview of the rubbing process and associated literature, the reader is referred to the very thorough review given by Muszynska [1]. Thermal effects, friction, impact, coupling, stiffening, analysis and vibrational response are included; the paper represents the first comprehensive review of the subject. Choy and Padovan [2] developed a general analytical rub model using the following assumptions: (i) simple Jeffcott rotor model, (ii) linear stiffness and damping characteristics, (iii) rigid casing supported by springs acting in the radial direction, (iv) mass inertia of the casing small enough to be neglected, (v) simple Coulomb friction and (vi) onset of rub caused by imbalance. Using the above assumptions, the rubbing period was categorized into four distinct processes: (a) non-contact stage, (b) rub initiation, (c) rub interaction and (d) separation.

The subject of sub-harmonic vibrational response was addressed by Ehrich [3]. Pseudo-critical responses at whole number multiples of the natural frequencies of a system are caused by non-linearities, typically due to asymmetry of radial stiffness in a rotor positioned eccentrically within its bearings. For instance, if a non-linear system has a natural frequency, ω, then pseudo-critical responses will be seen at forcing frequencies of 2ω, 3ω, 4ω, etc. A simplified, yet sufficiently descriptive, mathematical model was developed to verify predictions made about the behaviour of a real-life aircraft engine. Non-linear effects were introduced as a ratio of spring stiffnesses, within and beyond the total clearance, where equal stiffnesses constituted a linear system. A series of numerical simulations were performed, in order to examine the behaviour of the system under varying conditions of operating speed, damping and stiffness ratio. The simulated results agreed well with the conclusions made about the engine data. The same analytical model was also utilized by Ehrich [4] to study more closely the effects of chaos and subcritical superharmonic response in a system with rotor to stator contact. Again, real-engine data were supplied, against which the numerical results correlated with high accuracy. It was concluded that subcritical superharmonic response is the exact opposite of the previously discussed supercritical subharmonic response.

Goldman and Muszynska [5] reported that the study of system non-linearities, which cause chaotic motion to occur, is heavily dependent on the type of model used to simulate the impact stage of motion. Three general models were reported as having been used in the past for the analysis of rotor/stator impact: (i) a classical restitution coefficient-based approach; (ii) non-elastic impact with a zero restitution coefficient, where the impact is followed by a sliding stage; (iii) a discontinuous piecewise approach, with extra stiffness and damping terms included during the contact stage. In their paper, the impact stage was modelled according to the third method, under the assumption that contact occurred at the rotor modal mass location. Numerical simulations showed that the system exhibited orderly harmonic and subharmonic responses, as well as chaotic motion. Goldman and Muszynska [6] then used this model to investigate further, the effects of order and chaos in a system with contacting components. Results were supplied from a small experimental rig, able to simulate the presence of a loose bearing pedestal, as well as from an equivalent mathematical model. The two sets of results displayed characteristics of both orderly periodic and fully chaotic responses. For further

information, the reader is also referred to the papers of Choy *et al.* [7, 8] and Chu and Zhang [9, 10].

In the present study, attention is paid to the effects of torsion on the steady state response of a system experiencing rotor-to-stator contact, which, to the authors' knowledge, has not been studied in any previously reported work. It is considered that, to better understand the dynamical behaviour of such a system, not only lateral but also rotational motion must be taken into account. Under certain conditions to be determined, it is anticipated that the motion of an impacting mass acting against friction will be strongly influenced by the torsional properties of the system carrying that mass. This paper illustrates important differences in vibrational response between the models included in the above references, which include only lateral motion, and the below-described system, incorporating both lateral and torsional movement.

2. CONTACTING SYSTEM MATHEMATICAL MODEL

The analytical model utilized in this work is a development of the model given by Ehrich [3, 4]. This was considered a suitable starting point, since results obtained from simulations using this model were provided, which showed good correlation with previously reported experimental work by Bentley [11], and Muszynska [12], and with two different sets of real data collected from operational aircraft engines. The three-degrees-of-freedom Jeffcott rotor model, shown in Figure 1, was used for the present work.

The rotor is housed within the clearance of the stator: the rubbing phenomena of interest arise when contact occurs between these two sections, due typically to an initial unbalance excitation of the rotor. The stator local stiffness is taken as much higher than that of the rotor, and the degree of non-linearity in the system due to the effect of this piecewise spring is measured by the ratio of these stiffnesses, as shown in Figure 2.

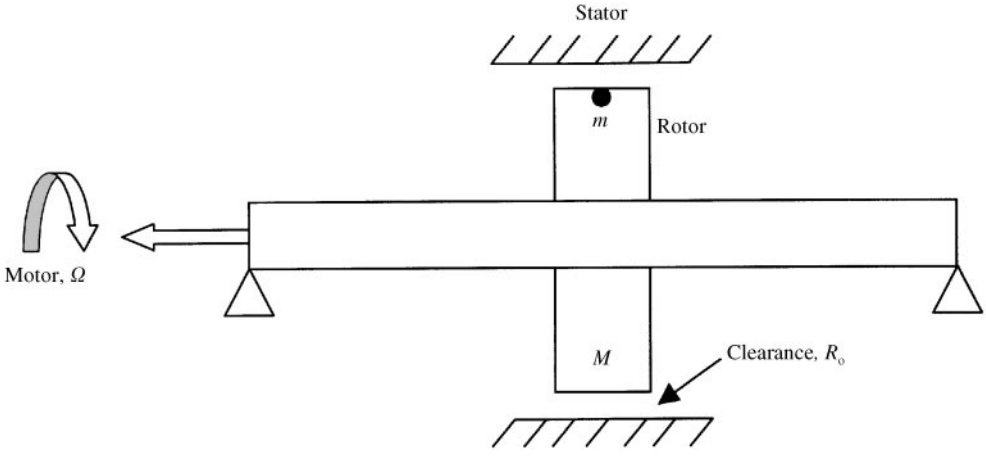

Figure 1. Jeffcott rotor model used for numerical simulations.

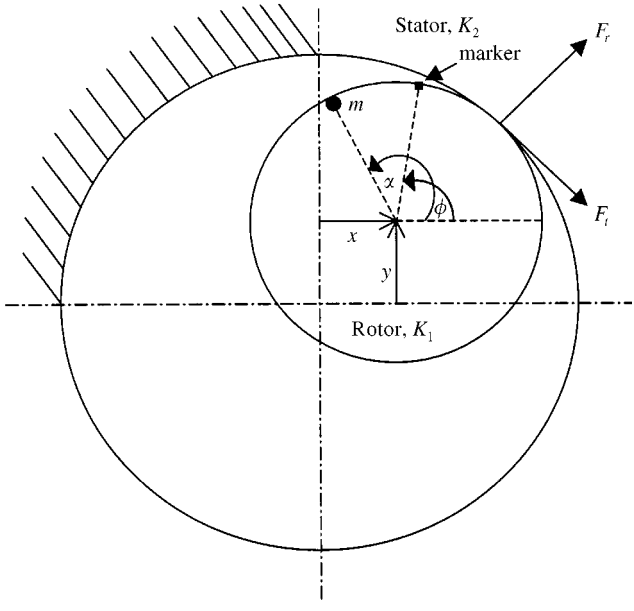

Figure 2. Contacting nonlinear rotor/stator system.

The equations of motion for the system, including lateral and torsional degrees of freedom, are as follows (all symbols defined in the Appendix):

$$M\ddot{x} + C_l\dot{x} = me\dot{\phi}^2\cos(\phi - \alpha) - me\ddot{\phi}\sin(\phi - \alpha) - F_x, \tag{1}$$

$$M\ddot{y} + C_l\dot{y} = me\dot{\phi}^2\sin(\phi - \alpha) - me\ddot{\phi}\cos(\phi - \alpha) - F_y, \tag{2}$$

$$J_d\ddot{\phi} + C_t(\dot{\phi} - \Omega) + K_t(\phi - \Omega t) = -aF_t, \tag{3}$$

where an overdot denotes differentiation with respect to time,

$$r = [(y - \delta)^2 + x^2]^{1/2}, \qquad F_r = rK_1 \quad (\text{for } r < R_0), \tag{4, 5}$$

$$F_r = R_0K_1 + (r - R_0)K_2 \quad (\text{for } r > R_0), \tag{6}$$

$$F_t = \mu(F_r - K_1r), \qquad F_x = F_rx/r + F_t(y - \delta)/r, \tag{7, 8}$$

$$F_y = F_r(y - \delta)/r + \delta K_1 - F_tx/r \quad (\text{for } \delta < R_0), \tag{9}$$

$$F_y = F_r(y - \delta)/r + R_0K_1 + (\delta - R_0)K_2 - F_tx/r \quad (\text{for } \delta > R_0). \tag{10}$$

The degree of system non-linearity is determined by the ratio of local stiffnesses of the rotor and stator, respectively, i.e.

$$\beta = K_1/K_2, \tag{11}$$

where equal stiffnesses ($\beta = 1$) below and above the clearance represent a fully linear system. Both flexural and torsional structural damping were included in damping ratio form: the higher value of stator stiffness, K_2, was used to calculate the damping ratio for lateral motion:

$$\zeta_t = \frac{C_t}{2\sqrt{K_t J}}, \qquad \zeta_l = \frac{C_l}{2\sqrt{K_2 M}}. \tag{12, 13}$$

At rest, the position of the rotor was taken as being displaced vertically by a value exactly equal to the clearance between rotor and stator in their axisymmetric positions. Then, for rotor displacement beyond the clearance, the higher stator stiffness, K_2, was used for contact in the vertical direction and the lower rotor stiffness, K_1, used in the horizontal direction. This condition causes the non-linear phenomena of interest to occur in the vertical direction. To investigate these phenomena, the system was analyzed numerically at pre-selected ratios of running speed to vertical natural frequency, where the natural frequency of the rotor/stator system with contact is

$$\Omega_2 = \sqrt{\frac{K_2}{M}}. \tag{14}$$

The ratio of vertical natural frequency to Ω_2 [3] is

$$\Omega_y = \frac{2}{(1 + \beta^{-1/2})}, \tag{15}$$

giving the running speed as

$$\Omega = s\Omega_2\Omega_y, \tag{16}$$

where, for example, s can be set to 1·00 for running speed at the first critical, or any multiples thereof.

Thermal effects have not been included in the analysis, for the sake of simplicity. Whilst the authors recognize the importance of heat production and heat transfer in rotor/stator contact, its inclusion at this stage would not benefit this particular study, since it is concerned solely with dynamic behaviour.

3. NUMERICAL SIMULATIONS

To judge the effect of including torsion in the mathematical model of the system, two sets of numerical simulations of an identical physical model were performed and the corresponding steady state responses obtained. Firstly, the response was calculated for lateral displacements only, by solving equations (1) and (2). A second

TABLE 1

Numerical model physical parameters

	Physical parameter	Value	Units
E	Young's modulus of elasticity	210·0	GN/m^2
G	Shear modulus of elasticity	79·6	GN/m^2
L	Shaft length	0·800	m
R_0	Clearance within stator	0·001	m
d	Shaft diameter	0·040	m
a	Disk radius	0·150	m
h	Disk thickness	0·030	m
$m.e$	Unbalance magnitude	25·0e-6	kg m
α	Unbalance phase angle	0·0	degrees
β	Non-linearity measure (stiffness ratio)	0·040	—
δ	Initial vertical displacement	0·001	m
ρ	Material density	7800·0	kg/m^3
μ	Coefficient of friction	0·50	—
ξ_t	Torsional damping ratio	0·01	—
ξ_l	Lateral damping ratio	0·01	—

set of results was then acquired, again by solving equations (1) and (2), and also including the torsional behaviour defined by equation (3). Realistic physical parameters, listed in Table 1, were selected for the model, to highlight the relevance of the study to real-life applications.

Runge–Kutta integration was applied to obtain the numerical solutions of equations (1)–(3) over the running speed range of 4–410 Hz, in 1 Hz increments ($0{\cdot}04 \leqslant s \leqslant 4{\cdot}00$), with 500 rotations at each step. A systematic study was carried out beforehand in order to verify that this number of rotations was sufficient to eliminate transient effects. More than double the number of rotations finally used were examined and this confirmed that, for the 1% lateral and torsional damping cases, 500 rotations were indeed sufficient to allow any transients to die away. In addition, only the data for the last 125 rotations was stored for post-processing.

To illustrate further the effect of torsion on rotor/stator contact, simulated results were obtained for varying torsional stiffness, whilst fixing the frequency ratio at a value of $s = 2{\cdot}5$. Relative Torsional Stiffness (RTS) was varied over the range $0{\cdot}01 \leqslant RTS \leqslant 5{\cdot}00$ where $RTS = 1$ corresponds to the torsional stiffness of the model having the parameters listed in Table 1. This range was deemed to include those values of torsional stiffness that would be obtained by varying the individual parameters of the rotor/stator system, such as the physical dimensions or material properties. Since the objective of this paper was to identify that there exists a difference between the responses returned by mathematical models considering only lateral motion, and those considering lateral and torsional motion together, a full parametric study was beyond the scope of the present work. The torsional stiffness was varied, however, in order to obtain an insight into the behaviour of the system, were these individual parameters to be altered.

4. RESULTS AND DISCUSSION

Bifurcation diagrams are a very effective means by which results obtained from systems exhibiting non-linear or chaotic behaviour may be presented, see reference [13]. These diagrams are constructed by plotting the response, y_t, at whole number multiples of the periodic time of the system in question, against the desired variable, where $t = mT$ ($m = 0, 1, 2, 3, \ldots$). In this way, periodic behaviour results in the repeated plotting of a single point (or points) over time, for each speed increment. Any non-periodic behaviour will result in multiple response values being plotted for the speed increment considered. Bifurcation plots are used to display non-linear and chaotic effects in systems encountered in many fields, such as population growth, plant-herbivore evolution and mechanical systems, to name just three.

Two bifurcation diagrams are presented in Figure 3, showing the calculated vertical displacement at each speed increment over the complete frequency range considered, for the two models without and with the inclusion of torsion respectively. In addition, orbit plots obtained at the four speeds $s = 1{\cdot}4$, $2{\cdot}5$, $2{\cdot}85$ and $3{\cdot}85$, are included for the two different solutions, to emphasize the differences between the two models.

At first glance, the two bifurcation plots appear to be alike; the results for the two different cases are comparable in terms of both their general shapes and their response magnitudes. Resonances occur at the natural frequency and whole number multiples thereof, which one would expect for a non-linear system of this kind. On closer examination, however, differences between the two sets of results become apparent. Firstly, in the range $0 < s < 1$, the response shown in plot(b) seems more stable than that shown in plot(a), where there is a wider scattering of points. Also, around the value $s = 1{\cdot}00$, the peak displayed in plot(b) is much more clearly defined than that in plot(a). Indeed, at $s = 1{\cdot}00$, there are at least 10 different recorded response values for plot(a), compared to 1 value for plot(b). In the range $1 < s < 2$, the response for the model without torsion once again seems less stable than its equivalent for the model with torsion. Moreover, three minor peaks at approximately $s = 1{\cdot}4$, $1{\cdot}6$ and $1{\cdot}7$ are evident in the torsional case, whereas there seems to be an almost random scattering of points in the purely lateral case. At $s = 2{\cdot}5$, a spike can be seen in the lateral model response, which is not present in the torsional case. For both models, there is a cluster of points around $s = 2{\cdot}6$, which is likely to be a chaotic, transitional stage between the second and third pseudo-critical resonances. These above-described disparities are liable to be due to energy interaction between angular and lateral motion, which is obviously not present if only lateral motion is considered. Torsional damping also has a part to play in the calculated system response and, although both the lateral and torsional damping ratios were fixed at 1%, this is a conceivable reason for the more settled behaviour of the model including torsion.

The trajectory plots included in Figure 3 serves to stress the importance of the study. For the two orbits displayed at $s = 1{\cdot}4$ (a frequency ratio coinciding with one of the smaller peaks of the torsional model), it can be seen that the two models exhibit wildly different results. The almost circular, periodic orbit shown in plot(a), which would not be unusual for a rotor operating near its first critical speed in

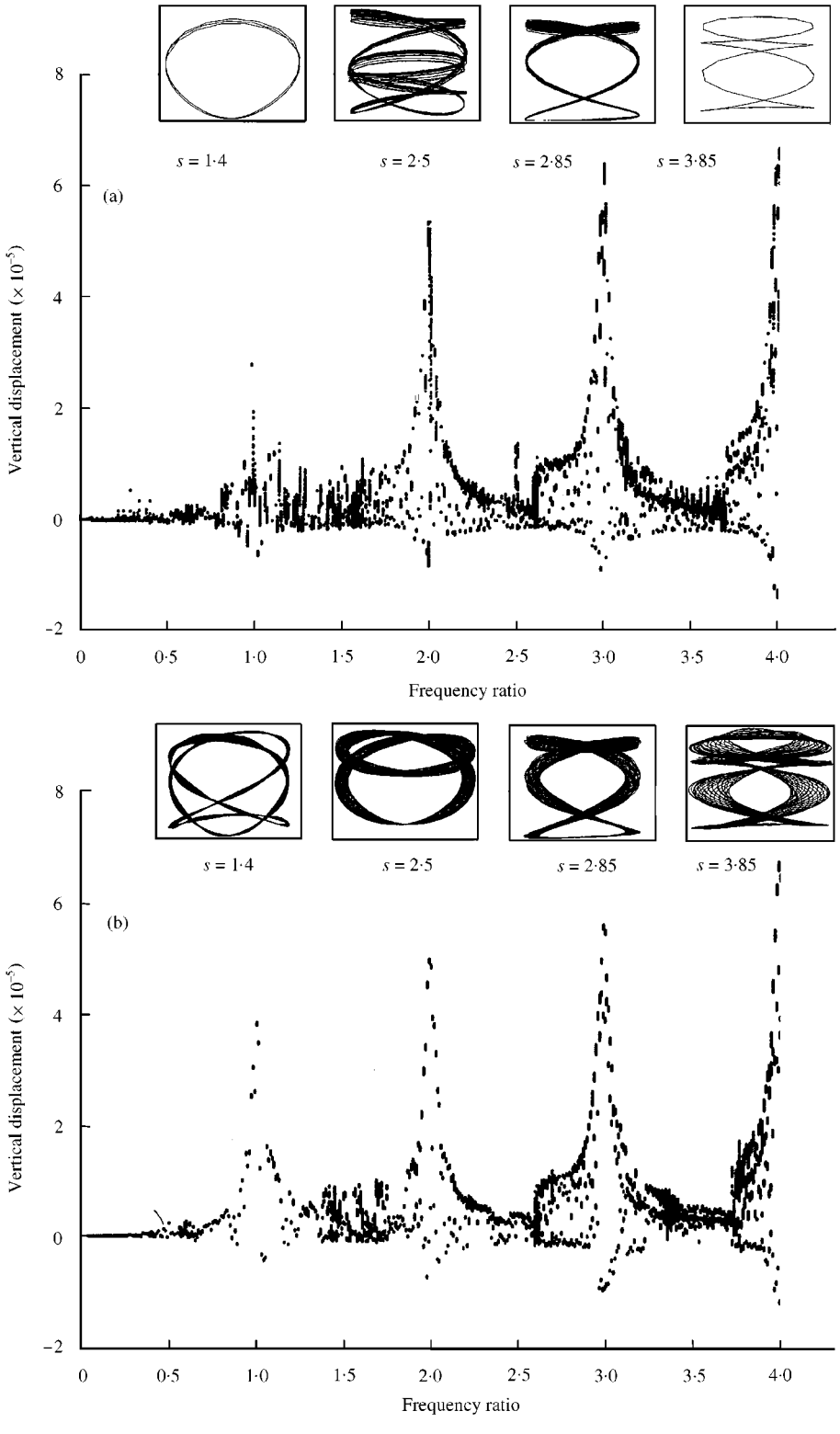

Figure 3. Bifurcation plots with varying frequency ratio; (a) without torsion; (b) with torsion.

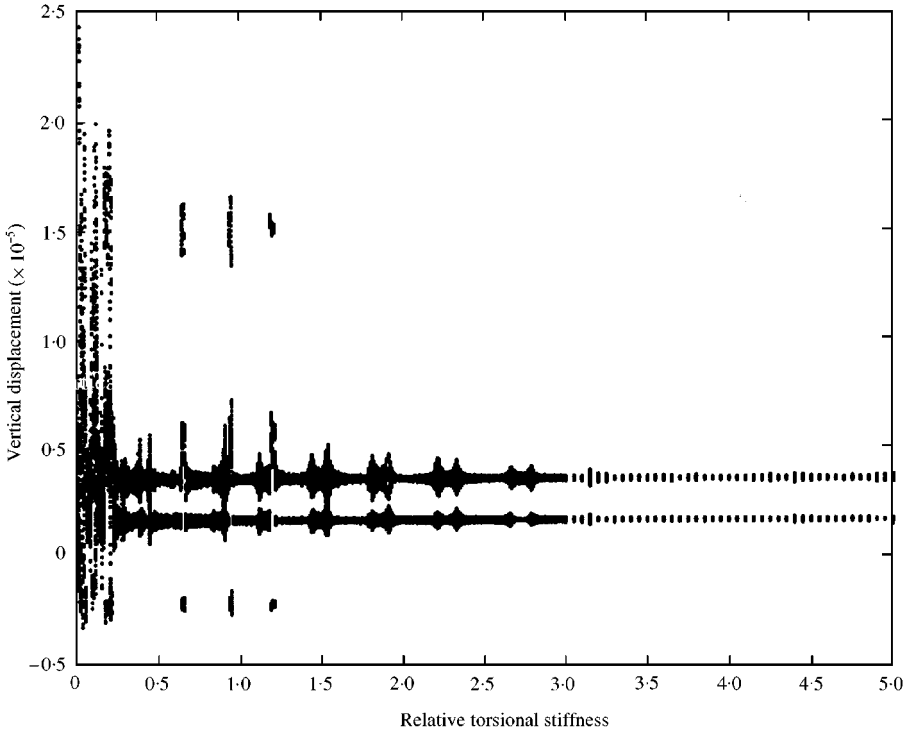

Figure 4. Bifurcation plot with varying torsional stiffness.

a linear system, is matched in plot(b) by a trajectory which, whilst periodic in nature (the pattern is repeated over many rotations), is non-linear and far from circular, although almost symmetric around the vertical axis. At $s = 2{\cdot}5$, the speed corresponding to the spike in Figure 3(a), the corresponding orbit for plot(a) appears to be chaotic in nature, particularly considering the highly periodic pattern of the next orbit shown for $s = 2{\cdot}85$. The orbit given in plot(b) for $s = 2{\cdot}5$, in contrast, follows a well-defined, but comparatively augmented, path. This again is most likely due to the energy interchange between lateral and torsional motion.

The trajectories in both cases, for $s = 2{\cdot}85$, are very similar. The basic form of the two plots is the same, only the trajectory in the torsional case once more follows a wider path. Like behaviour is again displayed for the trajectory plots taken at $s = 3{\cdot}85$. In plot(a), however, the path taken is periodic and exact: the same plot would be produced for just one period of rotation as for the 125 rotations used in these results. The general shape of this orbit is reproduced in plot(b). In this case, the orbit, whilst periodic, is much more spread out than for the case without torsion.

Figure 4 shows the bifurcation response obtained with varying the torsional stiffness and a fixed frequency ratio of $s = 2{\cdot}5$, where unity relative torsional stiffness corresponds to the initial model parameters used in the previous simulations. Firstly, it is important to note that the responses for the very low ($RTS < 0{\cdot}3$) and very high ($RTS > 3{\cdot}0$) torsional stiffness are what would be expected from such a variation in torsional stiffness. For the low torsional stiffness,

the response is widely scattered over a wide range of displacement values. The rotor is extremely flexible in torsion and such a rotor would seldom, if at all, occur in practice. For high torsional stiffness, the response tends to display a typical subharmonic response for a rotor running at over two times the first critical speed, i.e. two constant values of displacement are obtained for each periodic time increment. This same response is also obtained, as one would expect, at very high torsional stiffness, for example $RTS = 20{\cdot}0$. In the range $0{\cdot}3 < RTS < 3{\cdot}0$, some interesting phenomena are seen to occur. This range corresponds to those values that might be obtained by varying the individual parameters of the rotor/stator system, such as shaft or disk diameters, or material density. Clusters of points centred around the higher stiffness displacement values of about 0·16e-5, and 0·36e-5, appear in pairs and are spaced along the x-axis. Also, for values of RTS of approximately 0·66, 0·94 and 1·19, there are four main clusters visible. Investigation into the underlying cause(s) of these clusters and the reason(s) why, at certain stiffness values, there are four clusters instead of two, is beyond the scope of the current work. The aim of this research is to highlight the fact that the introduction of torsion into the mathematical model of a system experiencing rotor/stator contact does indeed have a considerable effect on the system behaviour. The differences in system response shown in Figure 4 serve to highlight this fact in a concise manner.

It is important to recognize from the results described above that certain parameters do exist where there will be very little difference between the responses exhibited by the two different models considered. However, taking into account all of the differences in the trajectory plots for the two cases and the bifurcation diagrams with respect to frequency ratio and relative torsional stiffness, it is clear that significant dissimilarity does exist between the responses obtained for the two models.

5. CONCLUSIONS

The effect of including torsion in the numerical analysis of a contacting rotor/stator system has been investigated. Two sets of data were obtained for the same physical model, with and without the inclusion of torsion. System response with respect to torsional stiffness has also been examined. The results presented show that, for a realistic physical system, periodic non-linear and also chaotic motion can occur. It may be concluded that torsion has a substantial effect on system response and should not be neglected in models used for the analysis of rub phenomena in rotating machinery.

REFERENCES

1. A. Muszynska 1989 *Shock and Vibration Digest* **21**, 3–11. Rotor to stationary element rub-related vibration phenomena in rotating machinery–literature survey.
2. F. K. Choy and J. Padovan 1987 *Journal of Sound and Vibration* **113**, 529–545. Non-linear transient analysis of rotor-casing rub events.

3. F. EHRICH 1988 *Journal of Vibration Acoustics Stress and Reliability in Design — Transactions of the ASME* **110**, 9–16. High-order subharmonic response of high-speed rotors in bearing clearance.
4. F. EHRICH 1992 *Journal of Vibration Acoustics—Transactions of the ASME* **114**, 93–100. Observations of subcritical superharmonic and chaotic response in rotordynamics.
5. P. GOLDMAN and A. MUSZYNSKA 1994 *Journal of Engineering for Gas Turbines and Power—transaction of the ASME* **116**, 992–701. Chaotic behaviour of rotor-stator systems with rubs.
6. P. GOLDMAN and A. MUSZYNSKA 1994 *Journal of Vibration and Acoustics – Transactions of the ASME* **116**, 541–547. Dynamic effects in mechanical structures with gaps and impacting: order and chaos.
7. F. K. CHOY, J. PADOVAN and W. H. LI 1988 *Mechanical Systems and Signal Processing* **2**, 113–133. Rub in high-performance turbomachinery, modelling, solution methodology and signature analysis.
8. F. K. CHOY, J. PADOVAN and W. QIAN 1993 *Journal of Sound and Vibration* **164**, 349–363. Effects of foundation excitation of multiple rub interactions in turbomachinery.
9. F. CHU and Z. ZHANG 1997 *International Journal of Engineering Science* **5**, 963–973. Periodic, quasi-periodic and chaotic vibrations of a rub-impact rotor system supported on oil film bearings.
10. F. CHU and Z. ZHANG 1998 *Journal of Sound and Vibration* **210**, 1–18. Bifurcation and chaos in a rub-impact Jeffcott rotor system.
11. D. E. BENTLEY 1974 *ASME Paper No.* 74-*Pet*-16. Forced subrotative speed dynamic action of rotating machinery.
12. A. MUSZYNSKA 1984 *3rd International Conference on Vibrations in Rotating Machinery, York, UK, Paper* C281/84, 327–335. Partial lateral rotor to stator rubs.
13. J. M. T. THOMPSON and H. B. STEWART 1986 *Nonlinear Dynamics and Chaos. New York; Wiley*

NOMENCLATURE

M	rotor mass
C	rotor damping
K_1	rotor stiffness
K_2	combined rotor and stator stiffness
J	polar moment of inertia
G	shear modulus of elasticity
E	Young's modulus of elasticity
F	force acting on rotor
R_0	clearance within stator
L	shaft length
T	periodic time
x	horizontal displacement
y	vertical displacement
r	radial displacement
m	unbalance mass
e	unbalance eccentricity
d	shaft diameter
a	disk radius
h	disk thickness
s	speed/frequency ratio
t	instantaneous time

Greek

ρ	material density
ϕ	rotational angle
α	unbalance phase angle
Ω	shaft running speed
δ	initial vertical displacement of rotor
ζ	damping ratio
β	non-linearity measure (stiffness ratio)
μ	coefficient of friction

Subscripts

l	lateral motion
t	angular (torsional) motion
x	horizontal direction
y	vertical direction
r	radial direction
d	referring to disk